

From Nodeless States and Vortices to Gray Rings and Symmetry-Broken States in Two-Dimensional Polariton Condensates

A.S. Rodrigues,¹ P.G. Kevrekidis,² R. Carretero-González,³ J. Cuevas,⁴ D.J. Frantzeskakis,⁵ and F. Palmero⁶

¹*Departamento de Física/CFP, Faculdade de Ciências,*

Universidade do Porto, R. Campo Alegre, 687 - 4169-007 Porto, Portugal

²*Department of Mathematics and Statistics, University of Massachusetts, Amherst MA 01003-4515, USA*

³*Nonlinear Dynamical Systems Group,* Department of Mathematics and Statistics,*

and Computational Science Research Center, San Diego State University, San Diego CA, 92182-7720, USA

⁴*Grupo de Física No Lineal. Departamento de Física Aplicada I. Escuela Politécnica Superior, Universidad de Sevilla, C/ Virgen de África, 7, 41011-Sevilla, Spain*

⁵*Department of Physics, University of Athens, Panepistimiopolis, Zografos, Athens 157 84, Greece*

⁶*Grupo de Física No Lineal. Departamento de Física Aplicada I. Escuela Técnica Superior de Ingeniería Informática, Universidad de Sevilla, Avda. Reina Mercedes, s/n, 41012-Sevilla, Spain*

(Dated: July 27, 2018)

We consider the existence, stability and dynamics of the nodeless state and fundamental nonlinear excitations, such as vortices, for a quasi-two-dimensional polariton condensate in the presence of pumping and nonlinear damping. We find a series of interesting features that can be directly contrasted to the case of the typically energy-conserving ultracold alkali-atom Bose-Einstein condensates (BECs). For sizeable parameter ranges, in line with earlier findings, the nodeless state becomes unstable towards the formation of *stable* nonlinear single or multi-vortex excitations. The potential instability of the single vortex is also examined and is found to possess similar characteristics to those of the nodeless cloud. We also report that, contrary to what is known, e.g., for the atomic BEC case, *stable* stationary gray rings (that can be thought of as radial forms of a Nozaki-Bekki hole) can be found for polariton condensates in suitable parametric regimes. In other regimes, however, these may also suffer symmetry breaking instabilities. The dynamical, pattern-forming implications of the above instabilities are explored through direct numerical simulations and, in turn, give rise to waveforms with triangular or quadrupolar symmetry.

I. INTRODUCTION

One of the most rapidly developing branch of studies in the physics of Bose-Einstein condensation is that of exciton-polariton condensates in semiconductor microcavities. Only a few years since their experimental realization¹⁻⁴, exciton-polariton Bose-Einstein condensates (BECs) have become a prototypical system for studies at the interface of non-equilibrium physics and nonlinear dynamics. More specifically, the radiative lifetime of the polaritons provides a short relaxation time scale in the system of the order of 1–10 ps⁵. At the same time, the light mass of these quasi-particles provides them with a considerably higher condensation temperature. Moreover, the photonic component of the system only allows for a short lifetime and no thermalization. Instead, the exciton-polariton system produces a genuinely non-equilibrium condensate, requiring the external pumping of an excitonic reservoir, which in turn balances the polariton loss^{5,6}. This “open” nature of the system, featuring gain and loss, is then responsible for its rich pattern forming capabilities that have been recently summarized, e.g., in Refs 7–9.

Our interest in the prototypical two-dimensional setting of the system will be precisely in the interplay of

the intrinsic nonlinearity due to inter-particle interactions and the gain/loss nature of the system. This interplay has led to a wide variety of remarkable observations (and theoretical explorations) including, but certainly not limited to, features such as flow without scattering (analogue of the flow without friction)¹⁰, the existence of vortices¹¹ (see also Ref. 12 for vortex dipole dynamics and Ref. 13 for observations thereof), persistent currents as well as higher charge vortices¹⁴, collective dynamics¹⁵, solitary wave structures such as bright¹⁶, dark¹⁷ and gap¹⁸ solitons, and even remarkable applications such as spin switches¹⁹ and light emitting diodes²⁰ operating even near room temperatures.

The approach that has been used most commonly in theoretical studies of exciton-polariton BECs relies on the analysis of two coupled evolution equations for the polaritons and the exciton reservoir which enables their production. In particular, the relevant model assumes the form of two coupled complex Ginzburg-Landau (cGL) equations describing the evolution of exciton and photon wavefunctions²¹⁻²³. However, an alternative that has been proposed^{9,24-26} in the case of incoherent and/or far blue-detuned laser pumping (see, e.g., Ref. 9 and references therein) suggests that a single cGL equation for the macroscopically occupied polariton state may be used instead; such a model yields results consistent with experimental observations²⁷ (see also Refs. 8,9).

In what follows, we will consider the case of incoherent pumping and use in our study a single cGL equation.

*URL: <http://nlds.sdsu.edu>

Our aim is to analyze in detail some of the fundamental states of the two-dimensional system. In particular, in earlier works these states have been chiefly obtained as attractors of the relevant gain/loss dynamics, revealing the pattern forming complexity that emerges spontaneously in the system. Here, our aim is not only to revisit fundamental states (such as the nodeless cloud or the single vortex) and explore their parametric dependence by developing two-parameter bifurcation diagrams (in parameters such as the gain strength and its spot radius); it is instead to provide a detailed view towards the stability of these states unveiling their spectral properties and the somewhat unusual nature of their instabilities. In addition to these more standard states, we will also consider states that, to the best of our knowledge, have not been previously presented in the context of polariton condensates, although they have been discussed for atomic condensates²⁸. A principal example of this form is the so-called ring dark soliton (RDS) which, remarkably, although never stable in the context of atomic BECs^{29–31}, can in fact be shown to be stable in suitable (gain) parametric regimes here. This is, effectively, a potentially stable radial form of a Nozaki-Bekki hole³² that was previously explored in cGL contexts³³, yet was not found to be stable in these settings; instead, it was found there to potentially initiate a form of spiral wave turbulence. We also reveal the symmetry-breaking instabilities of this ring structure and unveil a series of solutions without radial symmetry that may spontaneously emerge as a result of such instabilities. Among them, we highlight the potential for states with triangular or square/rectangular symmetry, whose parametric dependence (as stationary states) we also explore. Finally, for all relevant states, we offer a number of direct numerical simulations that yield insight towards the manifestation of the instabilities and the spontaneous emergence of patterns such as vortex lattices, but also of non-vortical patterns without radial symmetry. We should also note in passing here that a similar study focusing, however, predominantly on the existence properties of some of the solutions considered here (rather than on their stability, which is the principal emphasis herein), and chiefly considering the case without a parabolic trap, was recently published³⁴.

Our exposition is structured as follows. In section II, we offer the theoretical setup and techniques that will be used. In section III, we present the numerical results in two subsections: the first one provides the bifurcation structure and parametric continuations/stability analysis of the relevant solutions (initially this is done for the nodeless cloud and single vortex, and subsequently for the ring and related symmetry broken states); the second one examines the results of direct numerical results. Finally, in section IV, we summarize our findings, as well as mention some interesting directions for potential future studies.

II. MODEL SETUP

As indicated above, we will consider the complex Ginzburg-Landau model developed in Refs. 24–26 (see also Ref. 9 and references therein):

$$i\partial_t\psi = \{-\nabla_{\perp}^2 + r^2 + |\psi|^2 + i[(\chi(r) - \sigma|\psi|^2)]\}\psi, \quad (1)$$

where ψ denotes the polariton wavefunction trapped inside a two-dimensional (2D) harmonic potential, $\nabla_{\perp}^2 \equiv \partial_x^2 + \partial_y^2$ is the transverse (2D) Laplacian and $r^2 \equiv x^2 + y^2$ (note that the z -direction corresponds to the tight trapping axis). In fact, the above equation has the form of a “modified” Gross-Pitaevskii equation (GPE), which is the traditional lowest-order mean-field model describing atomic BECs^{35,36}: the differences of Eq. (1) from the traditional form of the GPE can be traced in the presence of (i) the spatially dependent gain term with

$$\chi(r) = \alpha\Theta(r_m - |r|), \quad (2)$$

where Θ is the step function generating a symmetric spot of radius r_m and strength α for the gain, and (ii) the nonlinear saturation loss term, of strength σ . Estimates of the relevant physical time and space scales, as well as physically relevant parameter values, are given, e.g., in Ref. 24. It is relevant to mention that although our results below are given in the context of Eq. (1), we have ensured that similar phenomenology arises in the model of Refs. 21–23, for suitable parametric choices. In that light, the phenomenology that is reported in this work should be *broadly* relevant to (2D) polariton BECs independently of model specifics. We also note in passing that Ginzburg-Landau-type models, similar to the one of Eq. (1) —i.e., including a localized gain term (but, in most cases, in the one-dimensional setting and without the external potential)— were recently studied in the context of nonlinear optics³⁷ and in the physics of magnon condensates³⁸.

In what follows, we will consider the stationary solutions of this 2D model, in the form $\psi(r, t) = \psi_0(r)\exp(-i\mu t)$ where μ is the dimensionless chemical potential, and the stationary state $\psi_0(r)$ is governed by the elliptic partial differential equation of the form:

$$\mu\psi_0 = \{-\nabla_{\perp}^2 + r^2 + |\psi_0|^2 + i[(\chi(r) - \sigma|\psi_0|^2)]\}\psi_0. \quad (3)$$

Importantly, an additional population balance constraint, i.e., an overall balancing of gain and loss within the 2D domain, has to be enforced: this condition is $dN/dt = 0$, where the norm $N = \int d^2r|\psi_0|^2$ depicts the number of polaritons. It is straightforward to show that the balance condition can be readily expressed as:

$$\int d^2r (\chi(r) - \sigma|\psi_0|^2)|\psi_0|^2 = 0. \quad (4)$$

It then follows that the above equation self-consistently selects the particular value of the chemical potential once the other parameters (i.e., α , σ , and r_m) are fixed. We

note in passing the significant difference of this trait from the Hamiltonian atomic BEC case, where there exist monoparametric families of solutions as a function of μ (which is a free parameter there rather than one dependent on the remaining gain/loss parameters).

Once stationary solutions of the differential-algebraic system of Eqs. (3)-(4) are identified, their linear (spectral) stability is considered by means of a Bogolyubov-de Gennes (BdG) analysis^{35,36}. Specifically, small perturbations (of order $\mathcal{O}(\delta)$, with $0 < \delta \ll 1$) are introduced in the form

$$\psi(x, y, t) = e^{-i\mu t} [\psi_0(x, y) + \delta p(x, y, t)], \quad (5)$$

with

$$p(x, y, t) \equiv a(x, y)e^{-i\omega t} + b^*(x, y)e^{i\omega^* t}. \quad (6)$$

Then, the ensuing linearized equations are solved to $\mathcal{O}(\delta)$, leading to the following eigenvalue problem:

$$\omega \begin{pmatrix} a(x, y) \\ b(x, y) \end{pmatrix} = \begin{pmatrix} L_1 & L_2 \\ -L_2^* & -L_1^* \end{pmatrix} \begin{pmatrix} a(x, y) \\ b(x, y) \end{pmatrix}, \quad (7)$$

for the eigenfrequency ω and associated eigenvector $(a(r), b(r))^T$, and L_1 and L_2 are the following operators:

$$L_1 = -\mu - \frac{d^2}{dx^2} - \frac{d^2}{dy^2} + r^2 + 2(1 - i\sigma)|\psi_0|^2 + i\chi(r),$$

$$L_2 = (1 - i\sigma)\psi_0^2.$$

When the eigenfrequencies are found to possess a positive imaginary part, then, per the ansatz of Eq. (6), an instability is expected to arise. On the other hand, if all the spectrum has $\text{Im}(\omega) < 0$, then the corresponding structure is spectrally stable. When a structure is found to be unstable, we conduct direct numerical simulations of Eq. (1) in order to explore the evolution of the instability and the state towards which the dynamics is attracted.

We now proceed to study the existence, stability and nonlinear dynamics of the different configurations of interest, namely the nodeless cloud, the single-charge vortex and the ring dark soliton-like waveform, as well as of some symmetry-breaking structures that result from the evolution dynamics of these states, when unstable.

III. NUMERICAL RESULTS

A. Existence and Spectral Stability

1. Nodeless Cloud and Central Vortex

We performed a search of nonlinear excitations for different values of the parameters. In what follows, we chose to keep $\sigma = 0.35$ (following the work of Ref. 39) fixed, and vary both the gain strength, α , and the gain spot

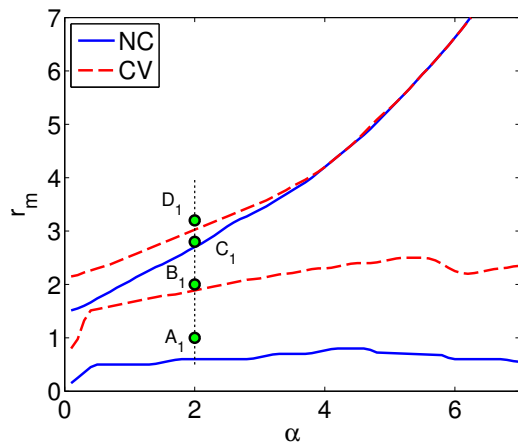


FIG. 1: (Color online) Stability domains of nodeless cloud (NC), and central vortex (CV) soliton-like solutions for $\sigma = 0.35$. The stable domains correspond to the regions between the curves. Circles indicate points shown in following figures for NC and CV solutions. All quantities shown here and in the figures that follow are dimensionless.

size radius, r_m , in order to develop two-parameter bifurcation diagrams characterizing the stability properties of the different states of interest. The relevant solutions were numerically obtained by using a (modified) Newton-Raphson method⁴⁸ in order to identify (and perform continuations on) solutions of Eq. (3), together with condition (4). This system forms a partial differential algebraic set of equations (PDAE).

We start by exploring the more fundamental solution profiles, namely the nodeless cloud (NC) and the central vortex cloud (CV).

It would be relevant to recall here, for comparison purposes, the stability properties of these waveforms in the Hamiltonian case of $\alpha = \sigma = 0$. There, the NC is the ground state of the system and is neutrally stable for all parameter values^{35,36}. Similarly, and although it is an *excited* state of the system (bearing an “anomalous” or “negative energy” mode), the CV is generically stable, independently of the chemical potential (or effectively the number of atoms) of the system⁴⁰.

The results of the scan of the parameter space are represented in Fig. 1, where we show the limits of stability of the NC and CV. Interestingly, it can be observed that while there are wide parametric regimes where the NC is stable, there are also large intervals of parameters where this solution is, in fact, unstable, contrary to what is known to be the case in atomic BECs. Furthermore, the stability region for the NC configuration is bounded both from above and from below, unlike the one-dimensional (1D) scenario of Ref. 39 where the stability region is only bounded above. Since there is loss everywhere, as the spotsize goes to zero there is only enough gain to sustain an ever smaller condensate, until it disappears in the limit of $r_m = 0$. On the other hand, also the CV

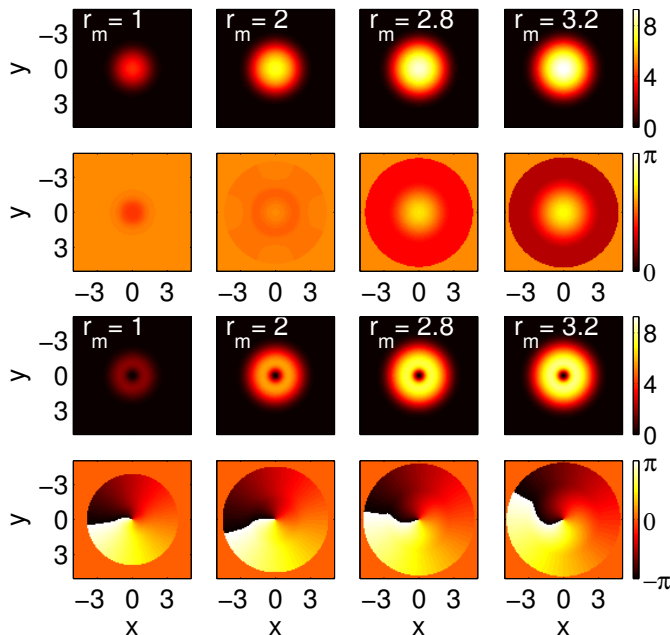


FIG. 2: (Color online) Density and phase profiles of nodeless cloud configurations (NC, top two rows) and central vortex configurations (CV, bottom two rows) for $\alpha = 2.0$ and $\sigma = 0.35$. The values of α and r_m used correspond, left to right, to points A₁-D₁ in Fig. 1.

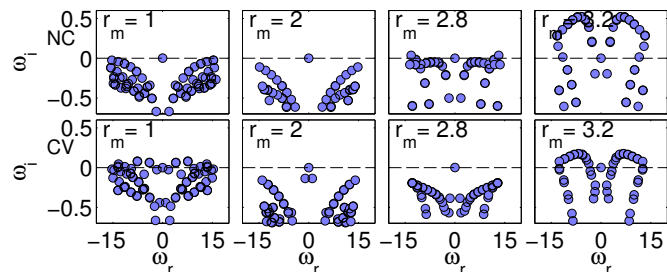


FIG. 3: (Color online) Eigenfrequencies ($\omega = \omega_r + i\omega_i$) associated with the spectral analysis of the NC (top) and CV (bottom) waveforms for the same parameter values as in Fig. 2.

features wide intervals of stability, but also ones of instability. It can, in fact, be seen that the feature identified as “stability inversion” in Ref. 39 for the case of 1D polariton BECs is still present here. Namely, there are regimes where the NC is stable but the CV is not, but also—in reverse—there are regimes where the CV is stable, but the NC is not.

In Fig. 2 we show the density and phase profiles of the NC (top two rows) and CV (bottom two rows) solutions for varying r_m . It is clear that as the radius of the drive increases, so does the size of the condensate. This is in contrast to what is the case with atomic BECs, where the size of the NC is controlled solely by the (parabolic)

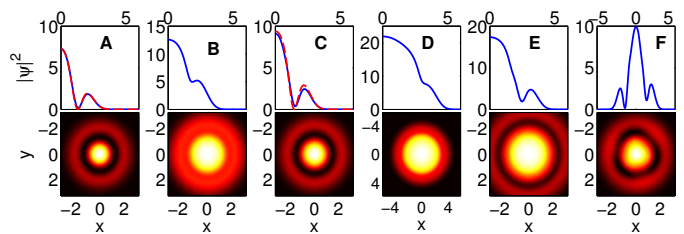


FIG. 4: (Color online) Profiles of gray rings (GR), and triangular solutions (TS) for the system parameters marked by (green) dots in the 2D plane of Fig. 5; $\sigma = 0.35$. Dashed (red) lines represent the Hamiltonian dark ring for the same chemical potential (panels A and C). Panel F represents a TS solution.

trap: here, the gain (and its interplay with the nonlinear loss/saturation) plays a critical role in the size of the waveform.

For the CV solutions of the bottom two rows, notice the characteristic 2π phase circulation. Similar features to the NC case are observed for the background on which the vortex “lives”.

We now turn to an examination of the stability of the different configurations. The spectral planes (ω_r, ω_i), where the subscripts r and i denote, respectively the real and imaginary parts of the eigenfrequency, for the NC and the CV configurations are illustrated in Fig. 3. There, it is evident that except for a weak instability arising through Hopf bifurcations for small values of r_m , for most intermediate values of r_m , both the NC and the CV configuration are stable. The predominant instability that arises for both configurations is the one for higher values of the gain r_m in this continuation. In that case, the instability arises in a less customary (for such structures, at least in their Hamiltonian form) way: entire segments of the continuous spectrum cross over the axis of $\omega_i = 0$ (see right panels of Fig. 3) and lead to bands of unstable eigenfrequencies. It is, thus, in a sense, perhaps expected that the entire “background state” of the system will be highly unstable towards a fundamentally different pattern, an expectation that indeed we will see to be confirmed by the direct numerical simulations featuring the instability evolution of these states.

2. Gray Rings and Triangular States

In addition to the more fundamental solutions explored above, we have identified a host of previously undisclosed, to the best of our knowledge, solutions of the 2D polariton BEC system. Arguably, the most remarkable among them is the so-called gray ring (GR) solitary wave, some typical density profiles of which are shown in Fig. 4. The depicted profiles correspond to the points shown as (green) dots in the 2D existence/stability (r_m, α)-plane (i.e., width and amplitude of the parametric gain) shown

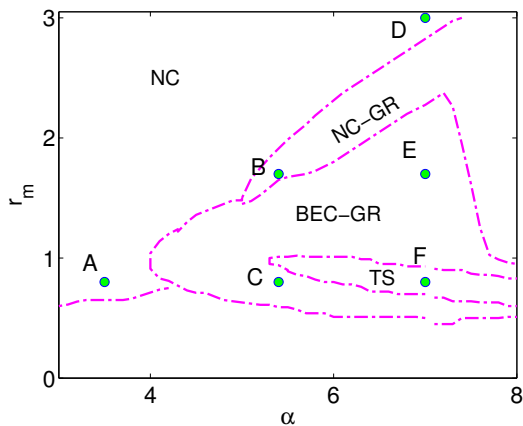


FIG. 5: (Color online) Existence domains of gray rings (GR), and triangular solutions (TS). Solutions are stable except that the GR is unstable where the TS exists. for $\sigma = 0.35$.

in Fig. 5. The plane itself reveals some of the interesting potential of such solutions, including the possibility of symmetry-breaking bifurcations giving rise to a new triangular form of solutions (denoted as TS). An additional remarkable feature is that while such ring dark solitons were proposed in both atomic condensates^{29–31} and in cGL gain/loss systems (as radial Nozaki-Bekki holes) in both contexts they were found to be unstable and thus break up into more prototypical coherent structures including vortices and spiral waves, respectively. We now turn to a more detailed examination of their properties including the existence and stability domains, also highlighting similarities and importantly differences from the above atomic case, including the generically gray nature of such excitations in our polariton setting.

For relatively low values of the gain spot size ($r_m < 1.3$) the GR can be either stable ($\alpha > 4.0$) or unstable. Above that value, the GR solution can only be identified within the parametric range indicated by the curves in Fig. 5. Interestingly, what is illustrated by the parametric plane is a progressive convergence of the GR and NC solutions, as represented by the label NC-GR in Fig. 5. This gradual “merging”, at the solution profile level, is signaled by the progressive increase of the phase variation of the NC until it reaches a value around π . Recall that from the results presented for the NC branch (Fig. 2), the phase varies by less than $\pi/2$. The admittedly somewhat arbitrary distinction between the NC branch and the GR one (and their hybrid NC-GR form) herein was based on whether there is a dip in the density profile (NC-GR) or not (NC). In particular, we observe that as the value of the gain grows, the NC becomes progressively more modulated.

On the other hand, there is an additional connection of such GR solutions with their BEC analogs discussed earlier in Refs. 29–31. In particular, as we approach the limit of weak and narrow drive ($\alpha \rightarrow 0$ and r_m small), the solution increasingly resembles the BEC ring dark

soliton (RDS) of the above works. This is illustrated in panels A and C of Fig. 4 where in addition to the polaritonic GR profile, the corresponding Hamiltonian case is also shown for the same chemical potential. As can be seen, the dip in both cases occurs at the same position, that is distinct from the gain spot radius. This (and the overall quality of the density comparison) is a strong indication of the origin of this solution from its corresponding Hamiltonian sibling. Recalling that the RDS in the Hamiltonian case is always unstable, we identify herein a critical role of the gain along with the saturating loss terms in inducing a limited region where this GR can be stabilized. As an addendum, it should be pointed out that the distinction between accordingly termed BEC-GRs and the previously discussed NC-GRs is obtained through the non-monotonic dependence of their dip versus the gain radius r_m . More specifically, for BEC-GRs, the depth of their dip (measured as the difference of the density at the center minus the density at the dip) is found to increase with increasing r_m , while NC-GRs are instead characterized by a decreasing dip (and NCs by a non-existent one). In reality, these solutions seem to seamlessly merge as the critical points identified are traversed, however, the above distinctions were given in order to better appreciate the “origin” of the different solutions.

An additional comment should be made here about the gray nature of these rings. Contrary to what is expected from their BEC siblings featuring a phase shift of π when stationary (and associated with a finite velocity when they are “gray”), in the polaritonic case, the rings are generically found to be gray. This is, in fact, reminiscent of what was recently found also in the context of complex \mathcal{PT} -symmetric potentials, e.g., in the work of Refs. 41, 42. In both cases, the origin of the phenomenon is the same: in particular, the complex nature (of the potential in the \mathcal{PT} -symmetric case and of the gain/loss structure in the cGL setting herein) of the terms in the equation produce a genuinely complex solution with a non-trivial phase structure and an associated “particle flux” along the stationary spatial profile. These features are absent in the BEC case, where the stationary RDS solution is genuinely real.

In passing we note that another GR-like solution we found, but that was never found to be stable, has its dip closer to the value of the gain spot size. It is therefore related to this length scale, contrary to what is the case for the GR solutions focused upon here. Due to the generic instability of the waveform apparently slaved to the gain, we do not explore it further here.

The spectral properties of the GR state have been found to be significantly different than those of the previous two fundamental states (NC and CV). In particular, as can be seen in Fig. 6, the instability of this state as r_m is increased stems from the fact that eigenfrequencies cross the origin of the spectral plane. This predisposes us towards a fundamentally different instability, possibly arising through a symmetry breaking pitchfork bifurca-

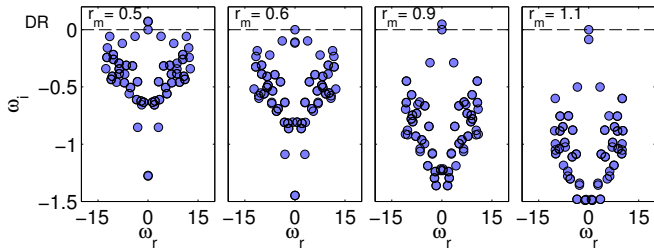


FIG. 6: (Color online) Spectra pertaining to the GR solution for $\alpha = 6.0$. Notice that for $r_m = 0.9$ the unstable GR solution coexists with a stable TS.

tion. We will see also how this expectation is manifested in the direct numerical simulations of the following section. This symmetry breaking bifurcation is substantiated in the parametric plane of Fig. 5 where a region has been denoted under TS (triangular solutions). As the curve outlining this region is crossed, the BEC-GR solutions undergo the above mentioned pitchfork bifurcation and spontaneously give rise to such TS. The TS states are generically found to be stable, a feature that will render them natural attractors for the BEC-GR unstable dynamics in the parametric range of TS existence, as will be corroborated in the dynamical evolution section below.

3. Quadrupoles

In the same spirit as the triangular solutions identified above, we have also been able to find solutions with quadrupolar symmetry. These solutions are especially relevant below the region of stability of the NC, as well as that of the (BEC-)GR. Such solutions are characterized by four dips of the density, at which location the phase portrait shows a winding of 2π (Fig. 8). This type of solution is also reminiscent of a corresponding quadrupole (vortex) solution in the realm of atomic BECs⁴⁰. In the latter setting, the solutions are critically induced by the parabolic trap, created from the linear limit thereof (as a complex combination of two of the second excited states of the 2D quantum-harmonic oscillator).

The regions of stability of the quadrupoles in the two parameter plane of (α, r_m) are shown in Fig. 7. Different classes of instability can be found, leading to exponential, oscillatory or combined decay. Nevertheless, islands of stability are also identified within which as we will see below the quadrupolar state can offer a dynamical attractor starting, e.g., from GR initial data, but also for both the NC and the CV.

As the gain strength grows, we find that the quadrupole exact solution profiles tend to a more elongated profile along a symmetry axis, reaching a form where the four dips nearly coalesce in two. Neverthe-

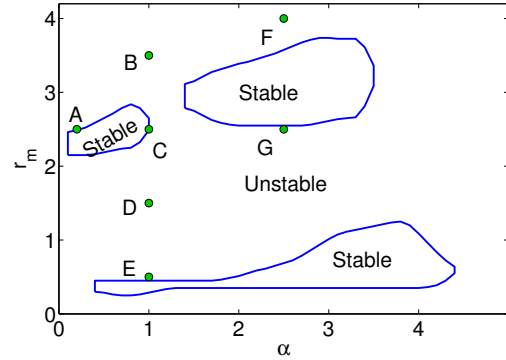


FIG. 7: (Color online) Stability domains of quadrupole solutions (QS), for $\sigma = 0.35$. The different letters denote case example profiles illustrated below in Fig. 8.

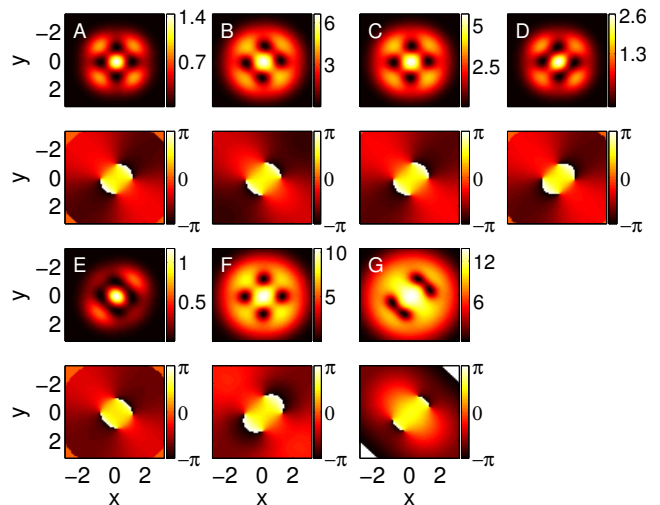


FIG. 8: (Color online) Density and phase profiles of quadrupole solutions (QS) for the values of α and r_m corresponding to points A-G in Fig. 7.

less, the phase (and the vorticity, not shown) reveal the four vortices of alternating positive and negative charge are still separate.

B. Dynamical evolution

As a way of confirming the stability results found above, and also of exploring the pattern forming outcomes of the dynamical evolution of the identified instabilities, we numerically integrated the full equation of motion, namely Eq. (1). Our initial conditions consisted of profiles in the form of the above obtained exact (up to a prescribed numerical tolerance) solutions, suitably perturbed to accelerate the decay, if unstable, or confirm that it returns to the attracting solution, if stable. The

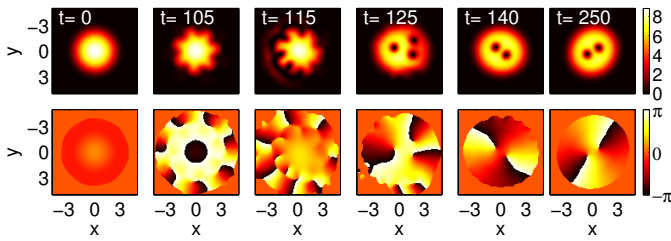


FIG. 9: (Color online) Dynamical evolution of a NC state for parameter values $\alpha = 2.0$ and $r_m = 2.8$, which is just outside of the stability region.

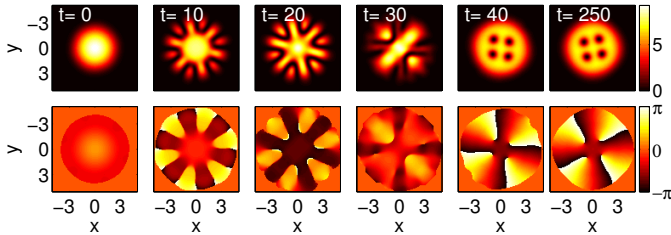


FIG. 10: (Color online) Dynamical evolution of a NC state for parameter values $\alpha = 2.0$ and $r_m = 3.2$. The resulting configuration of 4 vortices is rotating.

perturbation added for unstable waveforms was in the form of the profile of the eigenvector with the most unstable eigenfrequency. For the solutions expected to be stable, random noise was used. The latter results are not shown (they were only used to confirm the spectral stability results), but it was found that the solutions remained unaltered after propagation for time up to $t = 1000$.

Examples of the unstable scenarios are presented below. The results presented correspond again to points of the set A_1 - D_1 that are unstable (for each of NC and/or CV); other values lead to a qualitatively similar behavior. Figure 9 illustrates the case where the NC has just become unstable (for $r_m = 2.8$, while the stability boundary for this value of $\alpha = 2$ is $r_m = 2.7$). In this case, we can observe that the NC becomes unstable to an azimuthal modulation with eight-fold symmetry

and eventually, upon the nonlinear evolution of the instability, decays to a pair of rotating vortices. A further increase of $r_m = 3.2$ results in a similar evolution (cf. Fig. 10), but the end result is a rotating lattice of four vortices. Here we see a different initial symmetry in the dominant unstable mode (which appears to create a hexagonal modulation; see, e.g., the snapshots at $t = 10$ and $t = 20$), but also a nonlinear intermediate step in the evolution (see, e.g., snapshot at $t = 30$). It is naturally expected that, as r_m increases and the polariton condensate accordingly grows, more vortices can be “accommodated” therein, i.e., brought in the domain from the outside, and hence larger lattices created; this is in line also with the observations of Ref. 24. The evolution

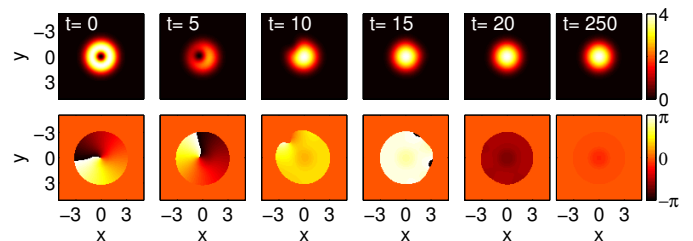


FIG. 11: (Color online) Dynamical evolution of a CV state for parameter values $\alpha = 2.0$ and $r_m = 1.0$, which is below its stability region.

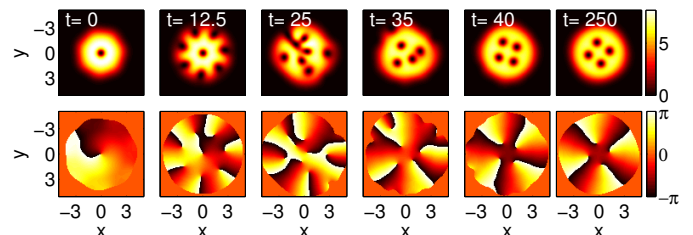


FIG. 12: (Color online) Dynamical evolution of a CV state for parameter values $\alpha = 2.0$ and $r_m = 3.2$, which is just outside (above) its stability region. The resulting configuration appears to ultimately lead to a rotating square (cf. Fig. 10 for the same parameter values).

typically starts with a modulation around the edge of the cloud that starts rotating. Comparison with the profile of the most unstable eigenvector suggests that the latter is indeed responsible for this (increasing) modulation. It eventually leads to one or more vortices spiralling (from the periphery) to the central region of the cloud until a stable and symmetric arrangement of vortices is achieved. The number of vortices (in the parameter range studied) can vary from one up to 21, either in a ring shape, with one more at the center, or as a lattice when their number grows.

The evolution of the CV solution features a similar behavior to the NC for parametric values beyond the upper stability boundary of this solution. In the region below the lower stability boundary, where the NC is generically stable, the CV typically decays to the NC (see, e.g., Fig. 11). Above the higher stability boundary of the CV solution, the vortex decays to a lattice of vortices as shown in Fig. 12. It is interesting to note that the original evolution of the instability results in more vortices within the cloud than the resulting asymptotic state, so there is a “distilling” process taking place, which finally results in the rotating square configuration observed at longer times (cf. for the same parameters, the asymptotically favored configuration of Fig 10).

We now turn to the dynamical results for the evolution of the GR solutions. Above its stability region, the GR typically decays towards the NC, which for this paramet-

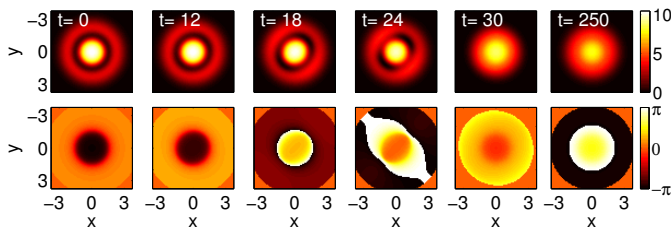


FIG. 13: (Color online) Dynamical evolution of a GR state for parameter values $\alpha = 4.2$ and $r_m = 1.3$, which is above its stability region. The final excitation is a NC state.

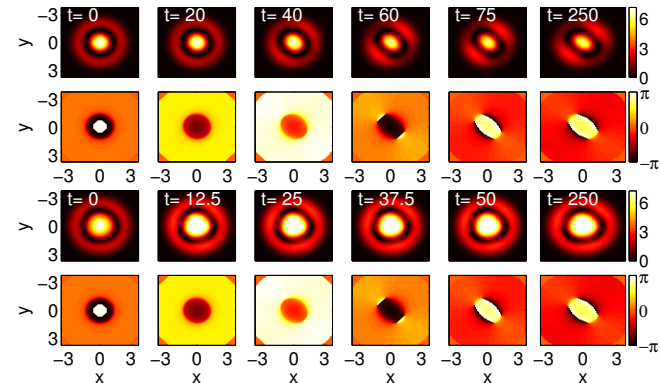


FIG. 14: (Color online) The top two rows show the dynamical evolution of a GR state for parameter values $\alpha = 4.2$ and $r_m = 0.7$, which is below its stability region. The final excitation features axial symmetry and is a QS. The bottom two rows show the dynamical evolution of a GR state for parameter values $\alpha = 6.9$ and $r_m = 0.8$, which is also outside its stability region. Here, however, the final excitation features triangular symmetry (TS).

ric region is well within its own range of stability in the (α, r_m) plane; this is shown, e.g., in Fig. 13, for $\alpha = 4.2$ and $r_m = 1.3$. In contrast, below the lower stability threshold of the GR, the latter may decay to different solutions depending on the exact parameters (and perturbations) used. An example of a relevant possibility is shown in the top two rows of Fig. 14 for $\alpha = 4.2$ and $r_m = 0.7$. This case reveals the possibility that the symmetry breaking instability of the GR (cf. the discussion of the previous section) may result into a quadrupolar configuration of the type explored in the previous section. On the other hand, the bottom two rows of Fig. 14 illustrate a different scenario for the parameter set $\alpha = 6.9$ and $r_m = 0.8$, which can be identified as being within the region of the symmetry breaking instability towards triangular solutions. In particular, the symmetry breaking spontaneously manifests itself dynamically resulting towards a configuration with triangular symmetry, as may be expected based on our existence/stability earlier findings. Solutions with this symmetry were previously identified in other contexts, e.g., Ref. 43. Nevertheless, these

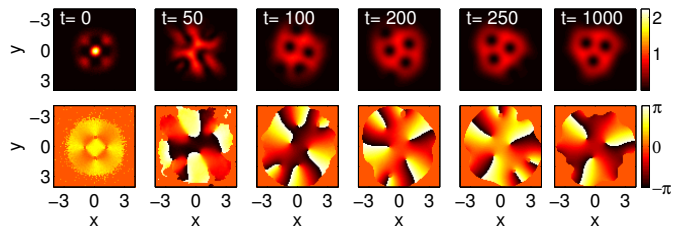


FIG. 15: (Color online) Dynamical evolution of a QS for parameter values $\alpha = 0.2$ and $r_m = 2.5$ (see point labeled A in Fig. 9). The final state is a rotating lattice of 3 vortices.

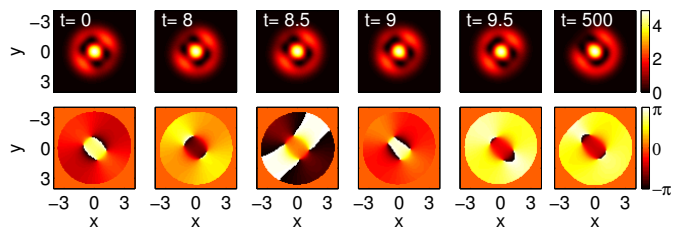


FIG. 16: (Color online) Dynamical evolution of a QS for parameter values $\alpha = 2.5$ and $r_m = 0.9$ (not in Fig. 9). It corresponds to an oscillatory instability.

results, and the absence of vortex lattice formation in this case, are in accordance with the results of the stability analysis of the GR presented above and its fundamentally different instability mechanism in comparison to the NC or CV configurations.

The evolution of the QS solutions shows a range of behaviors, from a decay towards a NC (for points D and G in Fig 7) to rotating lattices of vortices (A, B, C, and F). Among these, we highlight, in particular, the scenario A ($\alpha = 0.2$, $r_m = 2.5$), shown in Fig 15, where the final rotating cloud is highly distorted, as if more vortices were trying to join the 3 already in the central region of the cloud. It can also display an oscillatory instability, as in Fig 16, where the two dips at the extrema of the axial central lobe perform an oscillation, each pair with opposite phase than the other. Yet another situation is exemplified in Fig 17, where a lattice of vortices results, but unlike all other so far seen the inner vortices rotate at a different rate than the outer ones. Finally, the case F (see Fig. 18) results in a final excitation where a lattice with 7 vortices (one at the centre and an hexagon of vortices around it) rotates very slowly.

IV. CONCLUSIONS

In the present work, motivated by the intensely studied theme of polariton condensates, we offered a detailed view of the existence and stability, as well as the non-linear dynamical properties of some prototypical states

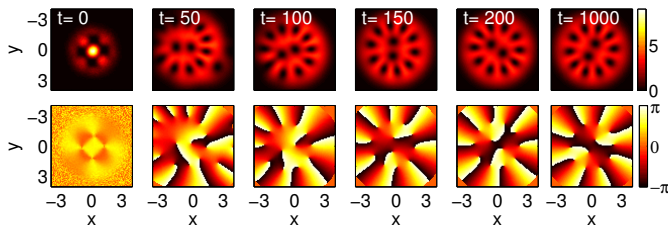


FIG. 17: (Color online) Dynamical evolution of a QS for parameter values $\alpha = 1.0$ and $r_m = 3.5$ (see point labeled B in Fig. 7). The final state is a rotating lattice of 10 vortices in a necklace plus 2 at the center. The two sets rotate at different rates. (Initial frame has its colormap scaled by a factor of $1/5$).

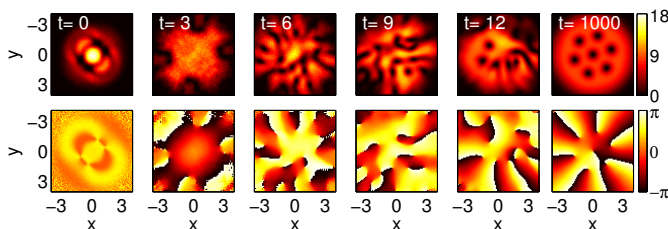


FIG. 18: (Color online) Dynamical evolution of a QS for parameter values $\alpha = 2.5$ and $r_m = 4.0$ (see point labeled F in Fig. 7). The final state is a (slowly) rotating lattice of 7 vortices. (Initial frame has its colormap scaled by a factor of $1/10$).

appearing in such systems. These states included fundamental earlier revealed waveforms such as the nodeless cloud (NC) and the cloud with a central vortex (CV). For these, we presented a systematic two-parametric analysis of their stability properties and how these are reflected in the corresponding nonlinear dynamics.

The fundamental (especially in the atomic BEC case) nodeless state was found to be stable only in a limited range of parameters. The most simple excited state, the central vortex state (which is again generically robust in atomic BECs), was found to, in fact, potentially exist as a stable object for parameters where the NC is no longer stable. Vice versa, the nodeless cloud was also stable in regimes where the vortex was not, presenting a 2D generalization of the stability inversions reported earlier in 1D counterparts of the model³⁹. Outside their stability ranges, they were both found to decay towards a series of rotating vortex lattices, in line with earlier numerical observations²⁴. However, here the precise (Hopf) nature of the instability was elucidated and the unusual associated morphology featuring the destabilization of an entire band of continuous spectrum eigenfrequencies was revealed.

As regards vortices, it should also be noted that we attempted to identify doubly charged vortex solutions, however, we were unable to obtain spectrally stable such

structures in the realm of the present model, i.e., such states were identified yet were always found to be dynamically unstable.

In addition to these simpler structures, we also explored more elaborate ones, especially in the form of a gray ring (GR) soliton-like structure, which was connected both to the NC but also to the ring dark soliton (RDS) state of atomic BECs. The inclusion of gain and loss in our complex Ginzburg-Landau-like equation was found to play a critical role in the potential stabilization of such ring states. Their generic gray structure was also justified by the flux induced by the gain/loss. Aside from identifying the stability islands of such GR states, their potential dynamical instabilities and associated bifurcations were also revealed. These were shown to lead to symmetry-breaking events generating (and asymptoting to) solutions of potentially triangular or quadrupolar structure. These states, in turn, were also identified as exact stationary solutions and their own two-parametric stability properties were explored.

A different set of gray ring structures was found but never stable, from what we could determine. This solution is mainly characterized by a central peak lower than the outer ring. It exists in regions in parameter space where other solutions exist stably. Thus for certain regions of parameters it is possible to find a NC, a GR and this other, always unstable gray ring.

All the results reported were for the parameter $\sigma = 0.35$, as stated before. Both from our previous results in the 1D setting, and from intuition and case examples considered, we expect that extending the continuation to other (nearby) values of σ should yield qualitatively similar results.

There are many directions towards which this exploration could further proceed. On the one hand, in the setting with the parabolic trap, it is interesting to explore the detailed stability of vortex clusters and progressively growing configurations towards vortex lattices. Understanding these clusters is still a very active area of research in atomic BECs⁴⁴; extending relevant (vortex) particle approaches (or distributional ones⁴⁵) in order to understand the properties and internal modes (in analogy to the Tkachenko modes of atomic BECs⁴⁶) of the system of a few or of many vortices, would be of particular interest in its own right. Yet another interesting direction, given the significant progress in imposing potentials of different kinds including periodic ones and identifying states critically supported by them (such as the gap solitons of Ref. 18), would be to explore the interplay of such clusters and lattices with external potentials and their structural phase transitions between different energetically preferred states as, e.g., the lattice parameters of an external periodic potential are varied⁴⁷. These and other related topics are presently under consideration and will be reported in future publications.

Acknowledgments

P.G.K. gratefully acknowledges support from the National Science Foundation, under grant CMMI-1000337, from the AFOSR under grant FA9550-12-1-0332, from the Binational Science Foundation under grant 2010239 and finally the warm hospitality of the IMA of the University of Minnesota and of KIP and the University of

Heidelberg during the final stages of this work. A.S.R. also acknowledges the hospitality of KIP and of the University of Heidelberg. The work of D.J.F. was partially supported by the Special Account for Research Grants of the University of Athens. J.C. and F.P. acknowledge financial support from the MICINN project FIS2008-04848.

-
- ¹ J. Kasprzak, M. Richard, S. Kundermann, A. Baas, P. Jeambrun, J. Keeling, F.M. Marchetti, M.H. Szymańska, R. André, J.L. Staehli, V. Savona, P.B. Littlewood, B. Deveaud, and L.S. Dang, *Nature* **443**, 409 (2006).
 - ² R. Balili, V. Hartwell, D. Snoko, L. Pfeiffer, and K. West, *Science* **316**, 1007 (2007).
 - ³ W. Lai, N.Y. Kim, S. Utsunomiya, G. Roumpos, H. Deng, M.D. Fraser, T. Byrnes, P. Recher, N. Kumada, T. Fujisawa, and Y. Yamamoto, *Nature* **450**, 529 (2007).
 - ⁴ H. Deng, G.S. Solomon, R. Hey, K.H. Ploog, and Y. Yamamoto, *Phys. Rev. Lett.* **99**, 126403 (2007).
 - ⁵ B. Deveaud (Ed.), *The Physics of Semiconductor Microcavities* (Wiley-VCH, Weinheim, 2007).
 - ⁶ *Exciton Polaritons in Microcavities, New Frontiers*, Springer Series in Solid-State Sciences Vol. 172, edited by D. Sanvitto and V. Timofeev (Springer, New York, 2012).
 - ⁷ H. Deng, H. Haug, and Y. Yamamoto, *Rev. Mod. Phys.* **82**, 1489 (2010).
 - ⁸ J. Keeling and N.G. Berloff, *Contemporary Phys.* **52**, 131 (2011).
 - ⁹ I. Carusotto and C. Ciuti, *Rev. Mod. Phys.* **85**, 299 (2013).
 - ¹⁰ A. Amo, J. Lefrère, S. Pigeon, C. Adrados, C. Ciuti, I. Carusotto, R. Houdré, E. Giacobino, and A. Bramati, *Nature Phys.* **5**, 805 (2009).
 - ¹¹ K.G. Lagoudakis, M. Wouters, M. Richard, A. Baas, I. Carusotto, R. André, L.S. Dang, and B. Deveaud-Plédran, *Nature Phys.* **4**, 706 (2008); see also for half-quantum vortices the work of K.G. Lagoudakis, T. Ostatnický, A.V. Kavokin, Y.G. Rubo, R. André, B. Deveaud-Plédran, *Science* **326**, 974 (2009).
 - ¹² M.D. Fraser, G. Roumpos, and Y. Yamamoto, *New J. Phys.* **11**, 113048 (2009).
 - ¹³ G. Roumpos, M.D. Fraser, A. Löffler, S. Höffling, A. Forchel, Y. Yamamoto, *Nature Phys.* **7**, 129 (2011); G. Nardin, G. Grosso, Y. Léger, B. Pietka, F. Morier-Genoud and B. Deveaud-Plédran **7**, 635 (2011); G. Tosi, F.M. Marchetti, D. Sanvitto, C. Antón, M.H. Szymańska, A. Berceanu, C. Tejedor, L. Marrucci, A. Lemaître, J. Bloch, and L. Viña, *Phys. Rev. Lett.* **107**, 036401 (2011).
 - ¹⁴ D. Sanvitto, F.M. Marchetti, M.H. Szymańska, G. Tosi, M. Baudisch, F.P. Laussy, D.N. Krizhanovskii, M.S. Skolnick, L. Marrucci, A. Lemaître, J. Bloch, C. Tejedor, and L. Viña, *Nature Phys.* **6**, 527 (2010).
 - ¹⁵ A. Amo, D. Sanvitto, F.P. Laussy, D. Ballarini, E. del Valle, M.D. Martin, A. Lemaître, J. Bloch, D.N. Krizhanovskii, M.S. Skolnick, C. Tejedor, and L. Viña, *Nature* **457**, 291 (2009).
 - ¹⁶ M. Sich, D.N. Krizhanovskii, M.S. Skolnick, A.V. Gorbach, R. Hartley, D.V. Skryabin, E.A. Cerda-Méndez, K. Biermann, R. Hey, and P.V. Santos, *Nature Photonics* **6**, 50 (2012).
 - ¹⁷ G. Grosso, G. Nardin, F. Morier-Genoud, Y. Léger, and B. Deveaud-Plédran, *Phys. Rev. Lett.* **107**, 245301 (2011).
 - ¹⁸ D. Tanese, H. Flayac, D. Solnyshkov, A. Amo, A. Lemaître, E. Galopin, R. Braive, P. Senellart, I. Sagnes, G. Malpuech, and J. Bloch, *Nat. Commun.* **4**, 1749 (2013); see also for a theoretical analysis of gap solitons in polariton condensates the recent work of E.A. Ostrovskaya, J. Abdullaev, M.D. Fraser, A.S. Desyatnikov, and Yu.S. Kivshar *Phys. Rev. Lett.* **110**, 170407 (2013).
 - ¹⁹ A. Amo, T.C.H. Liew, C. Adrados, R. Houdré, E. Giacobino, A.V. Kavokin, and A. Bramati, *Nature Photonics* **4**, 361 (2010).
 - ²⁰ S.I. Tsintzos, N.T. Pelekanos, G. Konstantinidis, Z. Hatzopoulos, and P.G. Savvidis, *Nature* **453**, 372 (2008).
 - ²¹ M. Wouters and I. Carusotto, *Phys. Rev. Lett.* **99**, 140402 (2007).
 - ²² M. Wouters, I. Carusotto, and C. Ciuti, *Phys. Rev. B* **77**, 115340 (2008).
 - ²³ C. Ciuti and I. Carusotto, *Phys. Stat. Sol. (b)* **242**, 2224 (2005).
 - ²⁴ J. Keeling and N.G. Berloff, *Phys. Rev. Lett.* **100**, 250401 (2008).
 - ²⁵ M.O. Borgh, J. Keeling, and N.G. Berloff, *Phys. Rev. B* **81**, 235302 (2010).
 - ²⁶ M.O. Borgh, G. Franchetti, J. Keeling, and N.G. Berloff, *Phys. Rev. B* **86**, 035307 (2012).
 - ²⁷ G. Tosi, G. Christmann, N.G. Berloff, P. Tsotsis, T. Gao, Z. Hatzopoulos, P.G. Savvidis, J.J. Baumberg, *Nature Phys.* **8**, 190 (2012).
 - ²⁸ D.J. Frantzeskakis, *J. Phys. A* **43**, 213001 (2010).
 - ²⁹ G. Herring, L.D. Carr, R. Carretero-González, P.G. Kevrekidis, and D.J. Frantzeskakis, *Phys. Rev. A* **77**, 023625 (2008).
 - ³⁰ T. Kapitula, P.G. Kevrekidis, and R. Carretero-González, *Physica D* **233**, 112 (2007).
 - ³¹ G. Theocharis, D.J. Frantzeskakis, P.G. Kevrekidis, B.A. Malomed, and Yu.S. Kivshar, *Phys. Rev. Lett.* **90**, 120403 (2003); G. Theocharis, P. Schmelcher, M.K. Oberthaler, P.G. Kevrekidis, and D.J. Frantzeskakis, *Phys. Rev. A* **72**, 023609 (2005).
 - ³² K. Nozaki and N. Bekki, *J. Phys. Soc. Jpn.* **53**, 1581 (1984); *Phys. Lett. A* **110**, 133 (1985).
 - ³³ M. Bazhenov and M. Rabinovich, *Phys. Lett. A* **179**, 191 (1993). M. Bazhenov, M. Rabinovich, *Physica D* **73**, 318 (1994).
 - ³⁴ E.A. Ostrovskaya, J. Abdullaev, A.S. Desyatnikov, M.D. Fraser, and Yu.S. Kivshar, *Phys. Rev. A* **86**, 013636 (2012).
 - ³⁵ C.J. Pethick and H. Smith, *Bose-Einstein condensation in dilute gases* (Cambridge University Press, Cambridge,

- 2002).
- ³⁶ L.P. Pitaevskii and S. Stringari, *Bose-Einstein Condensation* (Oxford University Press, Oxford, 2003).
- ³⁷ C.-K. Lam, B.A. Malomed, K.W. Chow, and P.K.A. Wai, *Eur. Phys. J. Special Topics* **173**, 233 (2009); C.H. Tsang, B.A. Malomed, C.-K. Lam, and K.W. Chow, *Eur. Phys. J. D* **59**, 81 (2010); F. Kh. Abdullaev, V.V. Konotop, M. Salerno, and A.V. Yulin, *Phys. Rev. E* **82**, 056606 (2010); V. Skarka, N.B. Aleksić, H. Leblond, B.A. Malomed, and D. Mihalache, *Phys. Rev. Lett.* **105**, 213901 (2010); Y.V. Kartashov, V.V. Konotop, and V.A. Vysloukh, *Europhys. Lett.* **91**, 34003 (2010); M.J. Ablowitz, T.P. Horikis, S.D. Nixon, and D.J. Frantzeskakis, *Opt. Lett.* **36**, 793 (2011); Y.V. Kartashov, V.V. Konotop, and V.A. Vysloukh, *Opt. Lett.* **36**, 82 (2011); D.A. Zezyulin, Y.V. Kartashov, and V.V. Konotop, *Opt. Lett.* **36**, 1200 (2011); M.J. Ablowitz, S.D. Nixon, T.P. Horikis, and D.J. Frantzeskakis, *Proc. Roy. Soc. London A* **467**, 2597 (2011); Y.V. Kartashov, V.V. Konotop, and V.A. Vysloukh, *Phys. Rev. A* **83**, 041806(R) (2011); M.J. Ablowitz, S.D. Nixon, T.P. Horikis, and D.J. Frantzeskakis, *J. Phys. A* **46**, 095201 (2013).
- ³⁸ B.A. Malomed, O. Dzyapko, V.E. Demidov, and S.O. Demokritov, *Phys. Rev. B* **81**, 024418 (2010).
- ³⁹ J. Cuevas, A.S. Rodrigues, R. Carretero-González, P.G. Kevrekidis, and D.J. Frantzeskakis, *Phys. Rev. B* **83**, 245140 (2011).
- ⁴⁰ S. Middelkamp, P.G. Kevrekidis, D.J. Frantzeskakis, R. Carretero-González, and P. Schmelcher *Phys. Rev. A* **82**, 013646 (2010); see also R. Kollár and R.L. Pego, *Appl. Math. Res. Express* **1**, 1 (2012).
- ⁴¹ V. Achilleos, P. G. Kevrekidis, D. J. Frantzeskakis, and R. Carretero-Gonzalez *Phys. Rev. A* **86**, 013808 (2012).
- ⁴² D.A. Zezyulin and V.V. Konotop *Phys. Rev. A* **85**, 043840 (2012).
- ⁴³ O.V. Borovkova, V.E. Lobanov, Y.V. Kartashov, and L. Torner, *Opt. Lett.* **36**, 1936 (2011).
- ⁴⁴ R. Navarro, R. Carretero-González, P.J. Torres, P.G. Kevrekidis, D.J. Frantzeskakis, M.W. Ray, E. Altuntaş, and D.S. Hall *Phys. Rev. Lett.* **110**, 225301 (2013).
- ⁴⁵ J.R. Anglin and M. Crescimanno, arXiv:cond-mat/0210063.
- ⁴⁶ I. Coddington, P. Engels, V. Schweikhard, and E.A. Cornell, *Phys. Rev. Lett.* **91**, 100402 (2003).
- ⁴⁷ H. Pu, L.O. Baksmaty, S. Yi, and N.P. Bigelow, *Phys. Rev. Lett.* **94**, 190401 (2005).
- ⁴⁸ The modification of the Newton-Raphson method consists in performing the (singular) Jacobian inversion by means of a LSQR method.